Nanoscale

Accepted Manuscript

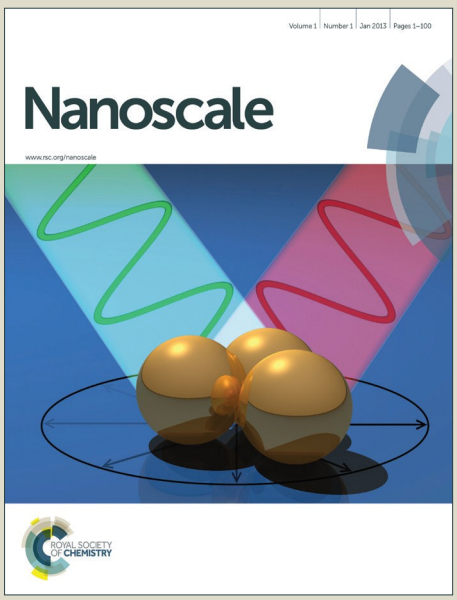

ROYAL SOCIETY OF CHEMISTRY

www.rsc.org/nanoscale

Nanoscale

ARTICLE

Effect of The Degree of Oxidation on Broadband Nonlinear Absorption and Ferromagnetic Ordering in Graphene Oxide

Received 00th November 2015,
Accepted 00th January 20xx

DOI: 10.1039/x0xx00000x

www.rsc.org/

Nikos Liaros,[a,b] Jiri Tucek,[c] Konstantinos Dimos,[d] Aristides Bakandritsos,[c,e] Konstantinos S. Andrikopoulos,[b,e] Dimitrios Gournis,[d] Radek Zboril[c]* and Stelios Couris[a,b]*

We report on the effect of degree of oxidation on the broadband non-linear optical response and magnetic behavior of graphene oxide, as well as on a route for obtaining reduced graphene oxide with enhanced optical properties without sacrificing the high dispersability of the parent graphene oxide. As more sp^3 states evolved with the rise in oxidation degree, it turned out that the sp^2/sp^3 fraction and sp^2 clustering are crucial parameters for tuning the broadband non-linear optical absorption over a wide range from ps to ns laser pulses from both visible and infrared laser irradiation. This was clearly confirmed by two different approaches, namely by a synthetic route through the gradual oxidation of graphene oxide from 1 to 3 oxidizing cycles, and reversely by *in situ* reduction of graphene oxide by UV laser irradiation. Furthermore, as sp^3 states carry localized magnetic moments, ferromagnetic ordering is observed at low temperatures. The magnetization and temperature at which ferromagnetic ordering evolves are found to increase with increasing the oxidation degree. The tuning of non-linear optical and magnetic properties of graphene oxide by oxidation/reduction thus provides an easy way to endow graphene oxide with tunable physical features highly required in both optoelectronics and spintronics applications.

Introduction

In recent years, the discovery of graphene, comprising a two-dimensional lattice of carbon atoms in a honeycomb arrangement,[1] has stimulated a huge interest in many scientific disciplines. More particularly, from the viewpoint of its optical properties, grapheme has already found a plethora of applications in photonics and optoelectronics, considered as a key material for the next generation optical devices.[2, 3] In this light, for the development of stable solid-state devices, there was a rapid growth of novel graphene-based two dimensional counterparts that show great dispersability and ease of preparation; the most well-known graphene derivative being graphene oxide (GO).[4] GO comprises a key functionalized analogue of graphene, displaying much more efficient dispersion in solvents and, therefore, much easier handling and applicability, and is thus widely considered as a precursor to graphene after its reduction.

On the way to implement GO in the realization and the development of integrated photonic devices,[5] considerable efforts have been dedicated for the investigation of its nonlinear optical (NLO) response, which has led to the discovery of some unique optical properties such as the broadband saturable absorption (SA) and the broadband optical limiting (OL).[6-8] In particular, in our group, we have previously studied in detail the NLO response of single and few layered GOs.[6, 9, 10] In all cases, GO dispersions were found to exhibit a large broadband optical power limiting action for both ns and ps pulse durations,[6] while few layered GOs were found to possess important and broadband optical limiting action under ns infrared laser wavelengths up to 1.8 μm, depending on the solvent used.[10]

GOs are layered semiconducting structures, featuring conducting π-states from the graphene sp^2 sites, and σ-states due to covalent bonding of oxygen groups to carbons.[11] The most important consequence of this mixture of hybridizations emanates from the offered possibility of tuning their optical band-gap in a controllable way, through the different amount of the induced sp^3 defects.[10, 12] Hence, it is reasonably expected that tuning of the energy gap provides a powerful strategy to tailor at-will the NLO properties of GO.[13] Moreover, the presence of sp^3 states featuring localized unpaired electrons in GO is believed to establish paramagnetic centres that may interact with each other via conducting π-delocalized electrons, promoting a potential evolution of a magnetically ordered state at low temperatures with a pure sp nature.[14]

[a] Department of Physics, University of Patras, 26504 Patras, Greece. E-mail address: couris@physics.upatras.gr
[b] Institute of Chemical Engineering Sciences (ICE-HT), Foundation for Research and Technology-Hellas (FORTH), P.O. Box 1414, Patras 26504, Greece
[c] Regional Centre of Advanced Technologies & Materials, Departments of Physical Chemistry and Experimental Physics, Faculty of Science, Palacky University, 17. listopadu 1192/12, 771 46 Olomouc, Czech Republic. E-mail address: radek.zboril@upol.cz
[d] Department of Materials Science and Engineering, University of Ioannina, 45110, Ioannina, Greece.
[e] Department of Materials Science, University of Patras, 26504 Patras, Greece.

†Electronic Supplementary Information (ESI) available: Preparation of the GO samples, experimental details of the Z-scan measurements, UV-Vis-NIR absorption spectra of the GO samples, and dynamic light scattering measurements. See DOI: 10.1039/x0xx00000x

Upon increase of sp^3, more paramagnetic centres emerge and the magnetically ordered state can be sustainable at high temperatures, a necessary prerequisite for applications in spintronics. However, the question of degree of oxidation on magnetic properties and their tuning has not been addressed so far, most probably due to different synthetic approaches used to prepare GO and difficulty to control systematically the oxidation degree. Moreover, the increase in sp^3 states in GO above the threshold level may disrupt communication between the paramagnetic centres and, hence, avoid establishment of the magnetically ordered state as sp^2 states, providing interaction medium, become less significant and weak to maintain interaction pathways.

In this work, we report on the effect of the oxidation extent on the broadband third-order NLO properties of GO prepared using a modified Staudenmaier method, employing visible (532 nm) and infrared (1064 nm), ps and ns laser irradiation. For this purpose, three different samples were prepared by the gradual oxidation of the GO from 1 to 3 oxidizing cycles ($GO_1 \rightarrow GO_3$), while XPS spectroscopy was employed to quantify the differences in the oxidation degree among the different GOs. The third-order NLO properties of GO dispersions as a function of the oxidation degree were determined by means of the Z-scan technique[15] and the nonlinear optical parameters were deduced. Reversely, *in situ* reduction of GO achieved by UV laser irradiation clearly confirmed the dependence of GOs' degree of oxidation on the NLO absorption, while, in all cases, the enhancement was quantified, highlighting the impact of UV-light reduction on the NLO response. In all cases, the variations in the oxidation degree of different dispersions were monitored *in situ* by Raman spectroscopy directly in colloidal state (aqueous environment). Moreover, with the rise in the number of sp^3 states upon oxidation, more paramagnetic centres with localized spins evolved. On lowering the temperature, the spins order ferromagnetically at the Curie temperature the value of which was observed to increase with the degree of oxidation. Furthermore, the magnetization in the low-temperature ferromagnetic state was found to increase with the rise of the oxidation level.

Experimental

Materials and methods

Sample preparation

Graphite (Fluka, 50870) was used as a starting material for the production of different GO samples. For the preparation of the GO dispersions, distilled H_2O was used (d.H_2O, 2 μS/cm) and NaOH (Sigma Aldrich, p.a. pellets). GO was synthesized using a modified Staudenmaier method and the preparation of the GO colloids was performed following our previous method.[6,9,10] Details of the preparation method for the samples are given in ESI†.

Characterization techniques

The concentration of the GO dispersions was determined with thermogravimetric measurements (TA instruments, Q500) under N_2 flow, by drying the solvent (H_2O) slowly up to 120 °C from a 100 μl sample and calculating the solid residue. The NaOH that was added in the solvent during the preparation of the colloids was taken into consideration.

Dynamic light scattering measurements (DLS) were performed with a ZetaSizer Nano Malvern instrument. Scattered light was collected at a fixed angle of 173°.

X-ray photoelectron spectroscopy (XPS) measurements were performed under ultrahigh vacuum conditions with a base pressure of 5×10^{-10} mbar in a SPECS GmbH instrument equipped with a monochromatic MgKα source ($h\nu$ = 1253.6 eV) and a Phoibos-100 hemispherical analyzer. Pulverized samples were dispersed in H_2O (1 wt%), and, after a short sonication and stirring, a minute quantity of the suspensions was drop cast on silicon wafers and left to dry in air before transfer to ultrahigh vacuum. The energy resolution was set to 0.3 eV and the photoelectron take-off angle was 45° with respect to the surface normal. Recorded XPS patterns were then averaged from 3 scans with an energy step set to 0.05 eV and a dwell time of 1 sec. All binding energies were referenced to the C1*s* core level at 284.6 eV. Spectral analysis included a Shirley background subtraction and peak deconvolution employing mixed Gaussian–Lorentzian functions, in a least squares curve-fitting program (WinSpec) developed at the Laboratoire Interdisciplinaire de Spectroscopie Electronique, University of Namur, Belgium.

Raman spectra were collected using two Raman setups. The 441.6 nm wavelength of a HeCd laser was used as the excitation source for the case of the HR-800 micro-Raman while the 632.8 nm wavelength of a HeNe laser was used as the excitation source for the second setup (T64000 micro-Raman). Both setups used single monochromators equipped with appropriate edge filters. The resolution was set at ~5 cm^{-1} in the spectral range recorded. The excitation beams (with a laser power of ~0.8 mW on a sample) were focused on the samples by a microscope objective (50x). All Raman spectra were recorded *in situ* from the GO aqueous dispersions. For the measurements, the GO aqueous dispersions were contained in 1 mm thick quartz cells.

The magnetic properties of the GO samples were assessed by recording the temperature dependence of magnetization employing a superconducting quantum interference device (SQUID)-type magnetometer (MPMS XL-7, Quantum Design, U.S.A.). The mass susceptibility, χ_{mass}, of the GO samples was measured in the sweep mode (1 K/1 min) in the temperature interval from 5 to 300 K under an external magnetic field of 1 kOe. The measured data were corrected assuming the signal of the sample holder and Pascal constants.

The third-order nonlinear optical (NLO) properties and the optical limiting (OL) performance of graphene oxide suspensions have been investigated with the Z-scan technique,[15] using a 35 ps mode-locked Nd-YAG laser and a 4 ns Q-switched Nd-YAG laser delivering visible (532 nm) and infrared (1064 nm) laser pulses. Details of the Z-scan method are described in the ESI†.

Results and discussion

Structural characterization

The C1s core level XPS patterns of the GO_1, GO_2, and GO_3 samples are shown in Fig. 1. As observed for the GO_1 sample, after deconvolution with mixed Gaussian–Lorentzian functions, the spectrum consists of five components. The main peak at 284.6 eV is attributed to the C-C bonds from the graphene sheet and contributes 49.8% of the total C1s intensity. The second peak at 285.8 eV (5.8%) is assigned to the C-O bonds of the hydroxyl functional groups, whereas the third component at 286.6 eV corresponds to the C-O-C epoxide/ether groups and represents 24.7% of the C1s intensity. The peak, recorded at a binding energy of 287.3 eV (8.3%), originates from the ketonic functionalities (C=O), while the peak at 288.8 eV (11.4%) is ascribed to the carboxyl groups (O-C=O).[16]

The XPS patterns of the GO_2 and GO_3 samples exhibit all the aforementioned peaks with an additional broad peak at 290.2-290.5 eV, which is associated with π-π* interactions.[16-18] However, the two spectra differ significantly compared to that of GO_1. As deduced by their % contributions to the total C1s intensities (see Fig. 1), the C-C bonds dominate in GO_1, C-O-C groups in GO_2, and C(O)O groups in GO_3.

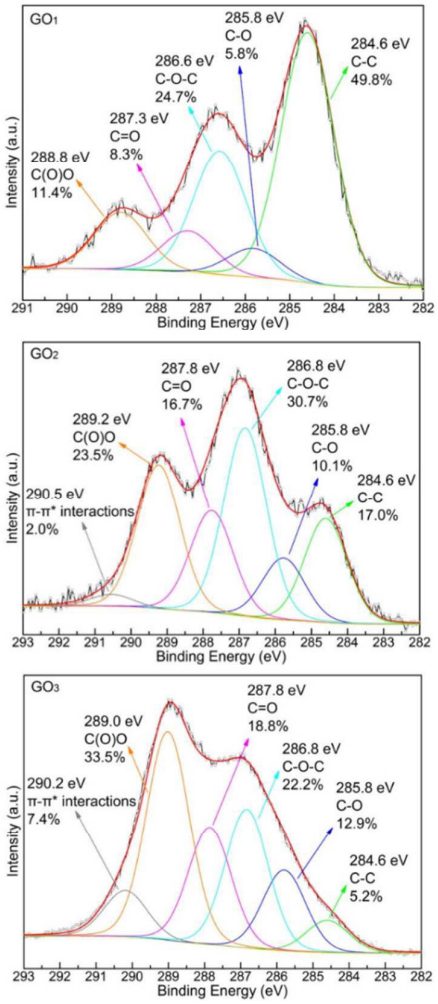

Fig. 1. C1s core level X-ray photoemission spectra of the GO_1, GO_2, and GO_3 samples.

Furthermore, it is obvious from the spectra overall shapes that upon oxidation, the formation of more oxidized groups is observed. The contribution of the oxygen functional groups of GO_1 to the total C1s intensity is ~50%. In the case of GO_2, the contribution of oxygen functional groups amounts to ~80%, while for GO_3, it reaches ~95%. In addition, the very low contribution (5.2%) of the C-C bonds to the total C1s intensity of GO_3 implies the extended oxidation of this material (see Table 1). In conclusion, XPS results clearly display the different oxidation states of the GO samples after one, two or three sequential oxidative treatments of graphite.

Table 1. Percentages of the bond types present in the three GO samples, as deduced from the recorded XPS patterns.

	C-C	C-O	C-O-C	C=O	C(O)O
GO_1	49.8	5.8	24.7	8.3	11.4
GO_2	17.0	10.1	30.7	16.7	23.5
GO_3	5.2	12.9	22.2	18.8	33.5

Nonlinear optical study: Effect of degree of oxidation on the broadband NLO response

For the NLO measurements, all samples were placed in 1 mm thick quartz cells. The relative UV-Vis-NIR spectra for GO_1, GO_2 and GO_3 aqueous dispersions are included in Fig. S1 in ESI†. The concentration of the different dispersions was adjusted as to exhibit the same optical density (OD) at the excitation wavelength (i.e., at 532 nm), which was set to be about 0.3. In order to attain the same measurable absorbance in the visible spectral region, the more oxidized the sample, the higher the concentration that was needed (see Fig. S1) because of the different extension of π-conjugation.[10] In Fig. 2, some representative "open-aperture" Z-scan recordings are presented for different dispersions, as obtained under visible and infrared, 35 ps and 4 ns laser excitation. The corresponding laser intensity that was used in each case is shown on the respective graph. Under all different excitation conditions, a clear dependence of the transmission minimum upon the degree of oxidation is manifested. More in detail, as the GO's oxidation gradually increases from GO_1 to GO_3, the transmission minimum in the "open-aperture" Z-scan decreases. As we have previously reported,[6] GO exhibits saturable absorption (SA) for low laser intensities switching to reverse saturable absorption (RSA) for higher ones; therefore, in order to determine the nonlinear absorption coefficient, β, the corresponding "open-aperture" Z-scans were fitted adopting an intensity dependent absorption coefficient, $\alpha(I)$, satisfying the relation in the form of[9]

$$\alpha(I) = \frac{\alpha_0}{1 + I/I_s} + \beta_{eff} I \qquad (1)$$

where the nonlinear absorption coefficient, β, relates to the two-photon absorption (TPA) or RSA occurring at high intensities, while I_s represents the saturation intensity related with the SA response. The continuous lines shown in Fig. 2a-d correspond to the best fitting of the "open-aperture" Z-scan transmission curves with the Eq. (1). It is important to notice that for 35 ps, 1064 nm excitation conditions, "open-aperture" Z-scan curves failed to be successfully fitted using the absorption coefficient described by Eq. (1) as evidenced by the continuous lines in Fig. 2d; in that case, it was required to adopt a different expression for the absorption coefficient, taking into account a four-photon absorption process, i.e.,

$$\alpha(I) = \frac{\alpha_0}{1 + \left(I/I_s\right)^3} + \beta \cdot I^3 \qquad (2)$$

and the dashed lines in Fig. 2d correspond to the best fittings using the above four-photon absorption model.

The determined values of β and the corresponding $\mathrm{Im}\chi^{(3)}$ for the three GO samples were found to decrease as the degree of oxidation increases ($GO_1 \rightarrow GO_3$) under all different excitation conditions, namely, visible and infrared ps and ns laser excitation. The β and $\mathrm{Im}\chi^{(3)}$ values for all the GOs are given in Table 2. It should be noticed that for the case of 35 ps, 1064 nm laser excitation, where Eq. (2) was employed to calculate the β parameter, the determined β values showed also similar trend and were found to

decrease with the oxidation increase, equal to 2.2, 0.6 and 0.3 × 10^{-41} m^5/W^3 for GO_1, GO_2 and GO_3, respectively.

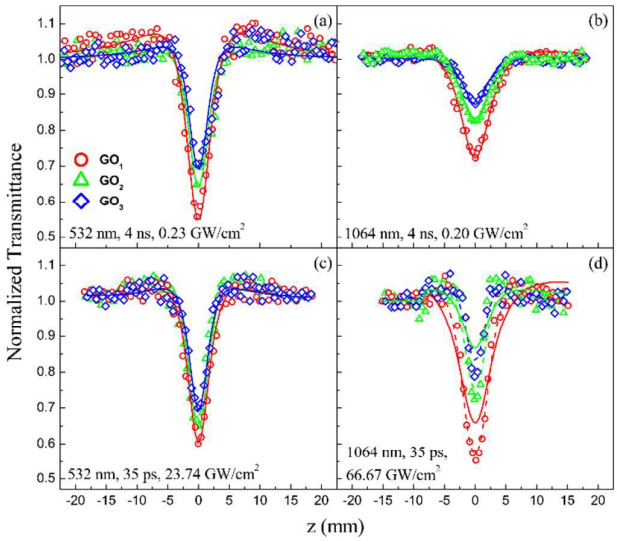

Fig. 2. "Open-aperture" Z-scans of the GO_1 GO_2 and GO_3 dispersions under 4 ns and 35ps, 532 and 1064 nm laser excitation. The solid and dashed lines correspond to the best fits of the experimental data using Eq. (1) and Eq. (2) respectively.

Table 2. Nonlinear Optical Parameters of GO.

τ	λ(nm)	sample	β [×10^{-9} cm/W]	Im$\chi^{(3)}$ [×10^{-13} esu]
35ps	532	GO_1	3.84±0.82	1.77±0.38
		GO_2	3.06±0.48	1.41±0.22
		GO_3	2.64±0.24	1.21±0.11
4ns	532	GO_1	148.82±14.14	68.44±6.50
		GO_2	104.08±28.07	47.87±12.91
		GO_3	65.64±19.80	30.19±9.11
		RGO_1	343±77 [a)]	158±35 [a)]
	1064	GO_1	46.44±6.26	43.87±5.91
		GO_2	30.18±7.08	28.51±6.69
		GO_3	20.18±5.62	19.06±5.31

[a)]Normalized with respect to the concentration of GO_3 (1.32mg/mL).

Effect of *in situ* reduction on the NLO response: A quantitative study

In order to extend our knowledge of GOs NLO absorption dependence on the degree of oxidation, we chose the most oxidized sample, i.e., GO_3, and performed *in situ* reduction by exposing the dispersions to UV laser irradiation, at the third harmonic of Nd:YAG (355 nm). For this purpose, GO_3 dispersions were homogenously irradiated at a fluence of 5 mJ/cm^2; the respective UV-Vis-NIR spectra are shown in Fig. 3. As can be clearly seen, by increasing the irradiation time, the absorption of GO gradually increases in the UV-Vis-NIR spectral region. After a certain time of irradiation (ca. 180 min), this increasing was found to reach a plateau, suggesting that GOs' reduction, at this particular irradiation fluence, had been accomplished (see Fig. 3a); the reduced sample was given the RGO_1 code name Next, the RGO_1 sample was further irradiated at a higher fluence (40 mJ/cm^2), and the absorbance increased even more, attaining a plateau after 150 min of irradiation; this second sample was named RGO_2 (see Fig. 3b).

Compared with the initial, highly oxidized GO_3 sample, the absorbance of the reduced RGO_1 and RGO_2 sample increased from 0.3 to 1.12 and to 1.43 at 532 nm, respectively. In order to perform the Z-scan measurements, the reduced samples were diluted so as to exhibit the same absorbance with the initial GO_3 (~0.3) at the excitation wavelength of 532 nm. In turn, dilution resulted in a much lower concentration for these dispersions with respect to the initial GO_3 ones, which were calculated to be about 0.35 mg/ml and 0.27 mg/ml for RGO_1 and RGO_2, respectively.

Interestingly, from the corresponding "open-aperture" Z-scan measurements that were performed under 4 ns, 532 nm excitation conditions, the nonlinear absorption coefficient, *β*, was determined to be about 66.28±16.68 and 70±15.78 for RGO_1 and RGO_2, respectively. These determined values are very close with that derived for GO_3 (65.64±19.80, see Table 2). However, one should notice the significant lower concentrations that were used for RGO_1 (0.35 mg/ml) and RGO_2 (0.27 mg/ml) dispersions compared to those used for the GO_3 ones (1.32 mg/ml), which confirms a significant enhancement of the NLO absorption owing to reduction process. In particular, the concentration ratios for the reduced samples with respect to the initial GO_3 were found to equal to 3.8 and 4.9 for RGO_1 and RGO_2, respectively. This implies that if the values are normalized with respect to the concentration, the nonlinear absorption coefficient, *β*, for RGO_2 would reach over 300 (Table 2).

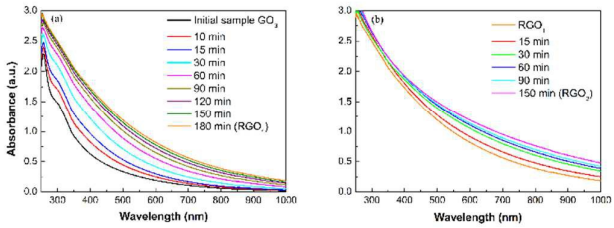

Fig. 3. UV-Vis-NIR absorption spectra of the reduced GO_3 dispersions (1.32 mg/mL) with (a) 5 mJ/cm^2 and (b) 40 mJ/cm^2, 355 nm laser irradiation.

Strikingly, the increase in NLO absorption after reduction through UV irradiation did not affect the colloidal stability, as normally expected for more reduced GOs.[19] In fact, the stability was preserved and even rather increased. This was clearly evidenced from the faster decay of the autocorrelation functions obtained by the DLS measurements of RGO_1 and RGO_2, in comparison to that of GO_3, as shown in Fig. S2 in ESI†. The faster decay should be ascribed to the smaller (and thus more stable) GO aggregates present in the dispersion. Therefore, the results suggest the development of a robust methodology leading to a product with a hybrid behavior, that shows a pronounced NLO absorption (typical for slightly oxidized samples), and, in addition, a high colloidal stability (characteristic of intensely oxidized GOs, such as GO_3).

Dependence of NLO response on the degree of oxidation: Monitoring the evolution of structural characteristics via *in situ* Raman spectroscopy

Concerning the NLO response of oxidized graphenes, the results that have been obtained in this work clearly show that the NLO absorption is greatly affected by the degree of oxidation. In

particular, it is shown that NLO of GO can be broadband tuned either by selectively changing the degree of oxidation by means of chemistry, or *in situ* through UV irradiation, by reducing the amount of oxygen groups on the GO sheet. It is also demonstrated that UV-reduction of the intensively oxidized GO_3 sample, can boost the NLO absorption to much higher values than the less oxidized samples (GO_1 and GO_2), but retaining the high colloidal stability of GO_3. In 2008, Li et al.[19] developed a chemical route employing hydrazine and ammonia in order to combine reduction with colloidal stability. The present route comes to establish an alternative chemical-free procedure for obtaining both colloidal stable RGO with pronounced NLO properties.

Raman spectroscopy is known to be a powerful tool for direct and nondestructive characterization of the structure and quality of carbon-based materials, particularly in order to determine defects, as well as ordered and disordered structures. However, in the majority of the reported works so far, Raman spectroscopy is employed in powder GO samples; in that case, the obtained information for the structural characteristics of the material is quite different than that of liquid environments, as in the case where Z-scan measurements are taken. Therefore, in order to shed more light in the relation that might hold between structural characteristics (e.g., sp^2/sp^3 ratio) and NLO response, we carried out Raman spectroscopy directly in the aqueous dispersions that were used for the nonlinear optical measurements. Raman spectra obtained from aqueous GO dispersions are plotted in the spectral region of the D and G bands in Fig. 4a. Several spectral features were found to alter as a function of oxidation and reduction processes. The most prominent change was seen with the fluorescence background which is stronger for the case of 632.8 nm excitation wavelength. Apart from the GO physicochemical properties, the fluorescent background depends on the concentration of the dispersion which might be slightly different for each sample. Therefore, for the compensation of the concentration factor and extraction of the fluorescence alteration caused by the physicochemical alteration of each sample, the ratio of the fluorescence intensity (at the frequency of the G band) divided by the Raman G band intensity was calculated. Fig. 4b correlates this ratio with the oxidation and reduction processes followed during sample treatment. As a result, the initially prepared GO exhibits considerable fluorescence which is furthermore moderately enhanced with subsequent oxidation increase. Furthermore, in accordance with other reports,[20-22] the reduction process employed in the current work leads to severe quenching of the recorded fluorescence, which further decreases with subsequent reduction steps.

Concerning the Raman spectroscopy, the I_D/I_G ratio is widely accepted as the most suitable quantity for the characterization of carbonaceous materials involves; it is proposed to be proportional to the defect concentration, only moderately depending on GOs' degree of oxidation, as shown in Fig. 4c. Interestingly, in our case, the I_D/I_G ratio is only slightly increasing during the oxidation process (at least, for the 632.8 nm set of measurements) and maintains its value approximately constant during the reduction. Almost equal I_D/I_G ratios for the reduced GOs could be related to the structural/distortion effects (e.g., surface rippling) that are formed on the graphene's lattice through the restoration of sp^2 bonding.[23] Furthermore, from our results, it is also manifested that the I_D/I_G ratio does not depend on the sample treatment (i.e., chemical synthesis or laser reduction) that has been employed in order to obtain GOs with different degree of oxidation. This observation is consistent with other reports, in which no significant variation of the I_D/I_G ratio was observed for reduced GOs with different degree of oxidation that were prepared either by hydro-thermal treatment,[22] or by annealing with varying temperatures up to 1000 °C.[24]

It is important to notice that the error bars in Fig. 4 indicate the variation of the I_D/I_G values calculated after performing different integration scenarios while the dissimilarity of the extracted I_D/I_G values for the two excitation wavelengths is typical since this ratio strongly depends on the excitation wavelength.[25] On the other hand, progressive alterations do take place at the frequency of the D and G band maxima as well as the associated full width at half maximum (FWHM) (see Fig. 4a). More specifically, the peak maxima appear to shift during oxidation process in a way that the frequencies of the band maxima approach one another, while they tend to abruptly diverge during the reduction process (see Fig. 4d). The most sensitive one is the G band whose maximum shifts by more than 30 cm^{-1} (441.6 nm) after the reduction of GO. While several studies have been performed for the dispersion of the D band, the position of the G band depends slightly on the structure, at least for the relatively/well-ordered carbon based materials (i.e., single wall carbon nanotubes, multi wall carbon nanotubes, graphene, graphite etc.).[26, 27]

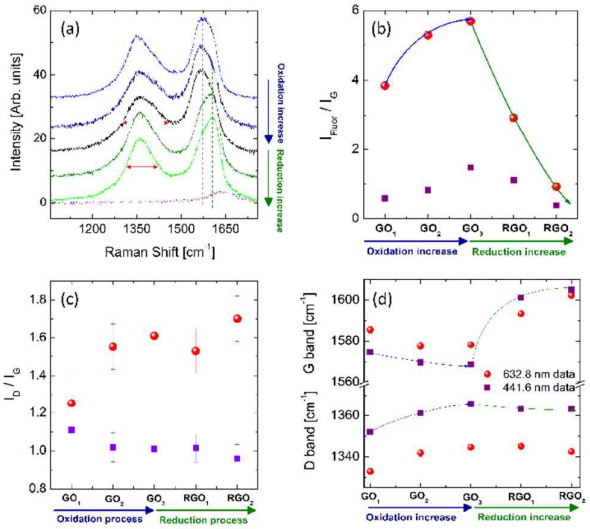

Fig. 4. (a) Raman spectra from aqueous GO dispersions using the 441.6 nm excitation wavelength. Notice the shift of the G band frequency (vertical dashed lines) as well as the alteration of the FWHM, especially for the case of the D band (arrows). Dashed spectrum at the bottom is obtained from pure water under the same experimental conditions as the GO suspensions. (b) The intensity ratio of the fluorescence background in the Raman spectra at the frequency of the G bands divided by the intensity of the G band for the differently oxidized/reduced samples. (c) Values of the I_D/I_G ratio for the differently oxidized/reduced samples (d). The frequency of the maximum of the D and G bands as a function of oxidation and reduction processes. Violet and red colored symbols in panels (b), (c), and (d) indicate experimental results using the 441.6 nm and 632.8 nm excitation wavelengths respectively. Lines are plotted as a guide to the eye.

One of possible physical parameters that influences the frequency of the G band in GO suspensions may be the number of stacking layers; however, since thorough and systematic experimental studies are required in this direction, we adopt another parameter

that has been proposed in an earlier study on the interpretation of the Raman spectra of disordered and amorphous carbon[28] and has been also implemented by Kudin et al.[29] as the most plausible explanation of the blue shift of the G band that they observed experimentally in their GO samples. In the above mentioned context, the shallow red shift of the G band is explained by the introduction of defects (sp^3) in the GO structure during the oxidation process, while the severe blue shift may be explained by the development of clustering of the sp^2 phase generated by the reduction process. As indicated by Ferrari and Robertson,[28] the quantification of the sp^3 content by Raman spectroscopy is particularly difficult, especially for the case of samples exposed to an ordering trajectory (formation of sp^2); probably, this is the reason why the I_D/I_G values do not appear to follow the general trend typically applied for well-ordered carbon based structures. Based on the above concept, we argue that the Raman spectra obtained *in situ* from GO suspensions indicate the generation of sp^3 species during oxidation process as well as the formation of sp^2 species in clustered phases during reduction process. This result is in perfect agreement with the results of our previous investigations concerning the NLO properties of few layered GOs[9, 10] under ns laser excitation, which showed larger NLO absorption than single layer ones, due to the extended π-conjugation that resulted from the increased amount of sp^2 localized nano-domains. Similarly, in ref. [7] it was reported that partial reduction of some GO thin films led to increased NLO absorption and optical limiting under fs laser irradiation, due to the increase of the sp^2 regions, while in ref. [13] studying some GOs with different number of layers, it was found that increase of the sp^2 regions (or equivalently decrease of the sp^3 regions), resulted to decrease of the optical limiting efficiency. In another work[30] studying the NLO response of some partial oxidized graphenes (sub-GOx) it was found that the NLO absorption could be significantly enhanced by increasing the number of π-electrons due to the increasing amount of sp^2 regions. On the basis of the present experimental evidences, it can be supported that the above mechanism is responsible for the broadband NLO absorption dependence on the oxidation degree, with the pulse durations extending from ps to ns regime. However, it should be realized that the nonlinear absorption might be expected to increase with the increase in oxidation when multiphoton absorption processes are dominant like under ps laser excitation (i.e., two- and four-photon absorption under 532 and 1064 nm respectively) since in that case, the sp^3 domains with the large energy gap of ca. 3 eV could explain the observed multi-photon resonances.[13] On the other hand, the fact should not be overlooked that the increase in the sp^2 domains with the subsequent decrease in oxidation could not only affect excited state absorption processes, such as RSA which is dominant under ns laser excitation, but also multiphoton processes.[7] Still, under visible (532 nm) ps excitation, the presence of RSA is also evident except from two-photon absorption, but infrared (1064 nm) ps excitation is rather negligible.

Effect of degree of oxidation on ferromagnetic ordering

In order to assess the magnetic properties of the GO samples with different degree of oxidation, the temperature evolution of magnetization was recorded, from which the profile of the mass susceptibility, χ_{mass}, was derived for each studied sample and the results are presented in Fig. 5. For all the three GO samples, the temperature behavior of χ_{mass} shows three common features: (i) an increase in χ_{mass} at low temperatures on cooling, (ii) a sign of local maximum in the temperature range between 20 and 50 K, and (iii) a decrease in χ_{mass} for temperatures above 50 K on warming. The decrease in χ_{mass} from 50 to 300 K can be well fitted employing the modified Curie-Weiss law, i.e., $\chi_{mass} = C/(T - \vartheta) + \chi_d$, where C is the Curie-Weiss constant, ϑ is the Weiss temperature, and χ_d is the diamagnetic susceptibility. It is known that pristine graphene with only sp^2 states behaves in a perfect diamagnetic manner.[14]

If some defects appear (such as vacancies, adatoms, edges, topology disorder, etc.), sp^3 states are introduced with emergence of localized magnetic moments. Thus, graphene and, hence, its derivatives may then behave paramagnetically or a magnetically ordered state can be established if the paramagnetic centers are close enough to each other so that below a certain temperature, a magnetic interaction is launched among them mediated by π electrons, as demonstrated previously in both theoretical and experimental reports.[14,31-34] As clearly seen from Fig. 5, χ_d is most significant for the GO_1 sample (like in pristine graphene) and is negligible for the GO_3 sample, indicating that with an increase in oxidation degree, more sp^3 states emerge leaving unpaired electrons as localized magnetic moments and, hence, forming paramagnetic centers.

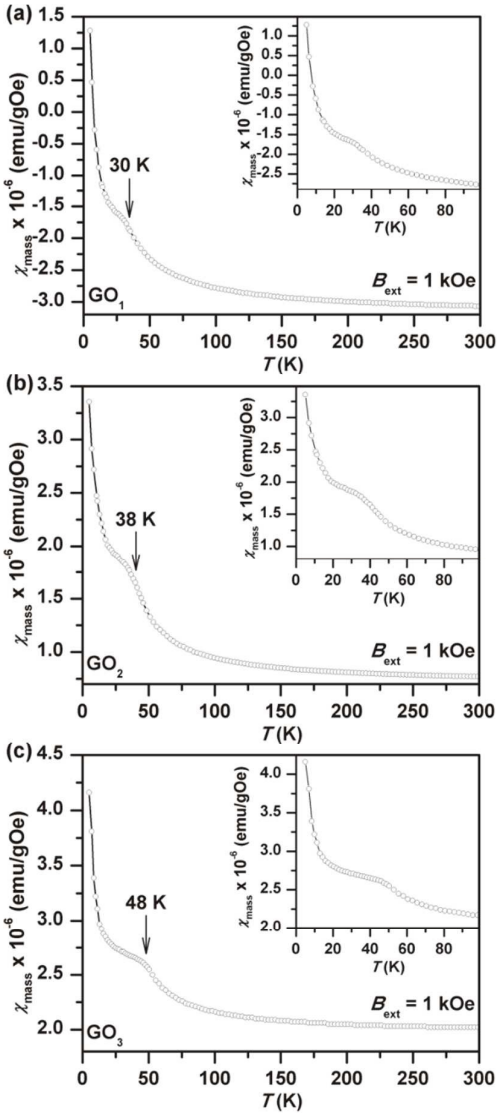

Fig, 5. The temperature evolution of the mass susceptibility (χ_{mass}), of the (a) GO_1, (b) GO_2, and (c) GO_3 sample, measured in the

temperature range from 5 to 300 K in an external magnetic field of 1 kOe. The insets show χ_{mass} profile at low temperatures.

The increase in a number of the paramagnetic centers upon oxidation is also witnessed from higher values of χ_{mass} at low temperatures (i.e., $\chi_{mass}(GO_3) > \chi_{mass}(GO_2) > \chi_{mass}(GO_1)$). As the temperature decreases, a sign a local maximum in χ_{mass} is observed implying a passage to a magnetically ordered state. From the χ_{mass} fitting, the Weiss temperature equals to ~30, ~38, and ~49 K for the GO_1, GO_2, and GO_3 sample, respectively. It is known that if $\vartheta > 0$, the magnetically ordered state is of ferromagnetic origin and ϑ can be assigned to the Curie temperature (T_C). It is then clearly seen that upon increase in the degree of oxidation, T_C increases. The low-temperature ferromagnetic ordering of the centers with localized spins in the GO samples is established via π delocalized electrons that migrate through the GO lattice and act as communicators among the paramagnetic centers. In other words, π delocalized electrons mediate the magnetic interaction between the magnetic moments localized at the formed sp^3 states; the magnetic interaction effectively develops only if the paramagnetic centers are sufficiently close to each other as the interaction decays with $1/r^3$ (r is the distance the π electron travels from one center to another). Once the paramagnetic centers are far separated they cannot magnetically communicate and stay lonesome exhibiting paramagnetic behavior down to 0 K. In all the samples, the presence of such paramagnetic centers is well documented by a further increase in χ_{mass} at temperatures from 20 to 5 K, perfectly obeying the simple Curie law (i.e., $\chi_{mass} = C/T$). In other words, at low temperatures, the GO samples contain paramagnetic centers that cooperate among each other in a ferromagnetic manner and paramagnetic centers that are isolated contributing to a paramagnetic signal down to very low temperatures. It is believed that a higher degree of oxidation might increase the number of paramagnetic centers and, hence, the probability of ferromagnetic behavior at higher temperatures. However, with the rise of sp^3 states upon oxidation, the number of π delocalized electrons may drastically decrease, limiting an evolution of the ferromagnetic regime over the whole GO lattice. Thus, a threshold level of oxidation is expected to promote an establishment of the ferromagnetic state with the highest T_C and strength; overcoming such a threshold oxidation degree would result in a collapse of the magnetic ordering and restoration of paramagnetic features down to very low temperatures.

Conclusions

In this work, we report on the effect of the oxidation degree on the magnetic properties and broadband third order NLO properties of GO, employing 35 ps and 4 ns laser irradiation. For this purpose, three different samples were prepared by the gradual oxidation of GO. The extent of oxidation among the different GO samples was quantified and verified with XPS technique and Raman spectroscopy. The third-order NLO absorption of GO dispersions as a function of the oxidation degree was determined by means of the Z-scan technique, and interestingly, under all different excitation conditions (i.e., pulse duration and excitation wavelength), it was found that lower oxidation leads to larger NLO absorption. Furthermore, *in situ* reduction of GO by UV laser irradiation clearly confirmed the dependence of GOs' degree of oxidation on the NLO response, since the reduced samples showed even higher NLO absorption than the initial, highly oxidized sample (GO_3). In both approaches, the evolution of the structural characteristics of the different dispersions that were imposed by the different amount of oxidizing species was monitored *in situ* by Raman spectroscopy directly employed in the colloidal state. The obtained results indicated the generation of sp^3 species during oxidation process as well as the formation of sp^2 species in clustered phases during UV reduction process. Therefore, it is evident that the extent of π-conjugation as quantified by the amount of sp^2 species arranged in nano-domains, plays a crucial role on GOs' broadband NLO absorption under both ns and ps laser excitation. Importantly, it was found that UV-reduction of the intensely oxidized GO_3 sample could boost the NLO absorption to very high values. At the same time, UV-reduction of GO_3 did not deteriorate the colloidal stability, as it would have been the case for conventional reduction routes of graphene oxides. The generation of more sp^3 states upon oxidation was further witnessed from temperature evolution of the mass magnetic susceptibility. The sp^3 states were identified to carry localized magnetic moments, behaving thus as paramagnetic centers. On lowering the temperature, paramagnetic centers were found to magnetically interact to establish the ferromagnetic ordering; the value of the Curie temperature and magnetic response in the ferromagnetic state increase with the degree of oxidation. It is speculated that if the degree of oxidation exceeds a threshold value, the ferromagnetic alignment can be lost restoring paramagnetic behavior over the whole GO lattice.

Acknowledgements

The smooth access to the Raman spectroscopic setups of the laboratory of applied molecular spectroscopy by Dr. G.A. Voyiatzis is greatly acknowledged. NL and SC acknowledge partial support by the European Union (European Social Fund–ESF) and Greek national funds through the Operational Program "Education and Lifelong Learning" of the National Strategic Reference Framework (NSRF)-Research Funding Programs: Heracleitus II and THALIS: Investing in knowledge society through the European Social Fund. JT, AB and RZ acknowledge the support by the Ministry of Education, Youth and Sports of the Czech Republic (LO1305).

Notes and references

1. K. S. Novoselov, A. K. Geim, S. V. Morozov, D. Jiang, Y. Zhang, S. V. Dubonos, I. V. Grigorieva and A. A. Firsov, *Science*, 2004, **306**, 666-669.
2. Q. Bao and K. P. Loh, *ACS nano*, 2012, **6**, 3677-3694.
3. F. Bonaccorso, Z. Sun, T. Hasan and A. C. Ferrari, *Nature Photonics*, 2010, **4**, 611-622.
4. D. R. Dreyer, S. Park, C. W. Bielawski and R. S. Ruoff, *Chemical Society reviews*, 2010, **39**, 228-240.
5. C. Yadav and S. Roy, *Journal of Computational Electronics*, 2014, **14**, 209-213.
6. N. Liaros, P. Aloukos, A. Kolokithas-Ntoukas, A. Bakandritsos, T. Szabo, R. Zboril and S. Couris, *The Journal of Physical Chemistry C*, 2013, **117**, 6842-6850.

7. X.-F. Jiang, L. Polavarapu, S. T. Neo, T. Venkatesan and Q.-H. Xu, *The Journal of Physical Chemistry Letters*, 2012, **3**, 785-790.
8. Z. Liu, Y. Wang, X. Zhang, Y. Xu, Y. Chen and J. Tian, *Applied Physics Letters*, 2009, **94**, 021902.
9. N. Liaros, K. Iliopoulos, M. M. Stylianakis, E. Koudoumas and S. Couris, *Optical Materials*, 2013, **36**, 112-117.
10. N. Liaros, E. Koudoumas and S. Couris, *Applied Physics Letters*, 2014, **104**, 191112.
11. G. Eda, C. Mattevi, H. Yamaguchi, H. Kim and M. Chhowalla, *The Journal of Physical Chemistry C*, 2009, **113**, 15768-15771.
12. K. P. Loh, Q. Bao, G. Eda and M. Chhowalla, *Nature chemistry*, 2010, **2**, 1015-1024.
13. Z.-B. Liu, X. Zhao, X.-L. Zhang, X.-Q. Yan, Y.-P. Wu, Y.-S. Chen and J.-G. Tian, *The Journal of Physical Chemistry Letters*, 2011, **2**, 1972-1977.
14. V. Georgakilas, J. A. Perman, J. Tucek and R. Zboril, *Chemical reviews*, 2015, **115**, 4744-4822.
15. M. Sheik-Bahae, A. A. Said, T. H. Wei, D. J. Hagan and E. W. Van Stryland, *IEEE Journal of Quantum Electronics*, 1990, **26**, 760-769.
16. R. Y. Gengler, D. S. Badali, D. Zhang, K. Dimos, K. Spyrou, D. Gournis and R. J. Miller, *Nature communications*, 2013, **4**, 2560.
17. V. Georgakilas, A. Demeslis, E. Ntararas, A. Kouloumpis, K. Dimos, D. Gournis, M. Kocman, M. Otyepka and R. Zbořil, *Advanced Functional Materials*, 2015, **25**, 1481-1487.
18. A. Kouloumpis, K. Spyrou, K. Dimos, V. Georgakilas, P. Rudolf and D. Gournis, *Frontiers in Materials*, 2015, **2**.
19. D. Li, M. B. Muller, S. Gilje, R. B. Kaner and G. G. Wallace, *Nature nanotechnology*, 2008, **3**, 101-105.
20. G. Xin, Y. Meng, Y. Ma, D. Ho, N. Kim, S. M. Cho and H. Chae, *Materials Letters*, 2012, **74**, 71-73.
21. G. Eda and M. Chhowalla, *Advanced materials*, 2010, **22**, 2392-2415.
22. C. H. Chuang, Y. F. Wang, Y. C. Shao, Y. C. Yeh, D. Y. Wang, C. W. Chen, J. W. Chiou, S. C. Ray, W. F. Pong, L. Zhang, J. F. Zhu and J. H. Guo, *Scientific reports*, 2014, **4**, 4525.
23. L. Zhang, E. Pollak, W.-C. Wang, P. Jiang, P.-A. Glans, Y. Zhang, J. Cabana, R. Kostecki, C. Chang, M. Salmeron, J. Zhu and J. Guo, *Carbon*, 2012, **50**, 5316-5322.
24. C. Mattevi, G. Eda, S. Agnoli, S. Miller, K. A. Mkhoyan, O. Celik, D. Mastrogiovanni, G. Granozzi, E. Garfunkel and M. Chhowalla, *Advanced Functional Materials*, 2009, **19**, 2577-2583.
25. M. A. Pimenta, G. Dresselhaus, M. S. Dresselhaus, L. G. Cancado, A. Jorio and R. Saito, *Physical chemistry chemical physics : PCCP*, 2007, **9**, 1276-1291.
26. M. S. Dresselhaus, A. Jorio and R. Saito, *Annual Review of Condensed Matter Physics*, 2010, **1**, 89-108.
27. Y. Wang, D. C. Alsmeyer and R. L. McCreery, *Chemistry of Materials*, 1990, **2**, 557-563.
28. A. Ferrari and J. Robertson, *Physical Review B*, 2000, **61**, 14095-14107.
29. K. N. Kudin, B. Ozbas, H. C. Schniepp, R. K. Prud'homme, I. A. Aksay and R. Car, *Nano Lett*, 2008, **8**, 36-41.
30. G.-K. Lim, Z.-L. Chen, J. Clark, R. G. S. Goh, W.-H. Ng, H.-W. Tan, R. H. Friend, P. K. H. Ho and L.-L. Chua, *Nature Photonics*, 2011, **5**, 554-560.
31. H. S. S. R. Matte, K. S. Subrahmanyam and C. N. R. Rao, *The Journal of Physical Chemistry C*, 2009, **113**, 9982-9985.
32. Y. Wang, Y. Huang, Y. Song, X. Zhang, Y. Ma, J. Liang and Y. Chen, *Nano Lett*, 2009, **9**, 220-224.
33. Y. Liu, N. Tang, X. Wan, Q. Feng, M. Li, Q. Xu, F. Liu and Y. Du, *Scientific reports*, 2013, **3**, 2566.
34. Y. Matsumoto, M. Koinuma, S. Ida, S. Hayami, T. Taniguchi, K. Hatakeyama, H. Tateishi, Y. Watanabe and S. Amano, *The Journal of Physical Chemistry C*, 2011, **115**, 19280-19286.

Nanoscale

ARTICLE

Table of Contents (TOC) Image:

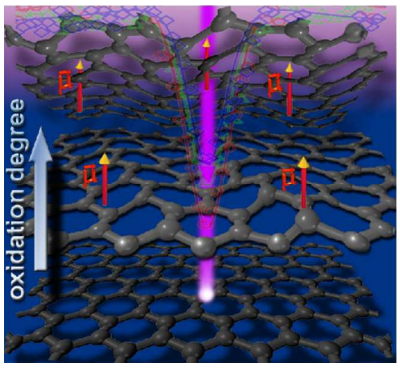

Electronic Supplementary Information (ESI)

1. Sample preparation

Graphene oxide (GO) was synthesized using a modified Staudenmaier method.[S1] 1 g graphite (Fluka, 50870) was dispersed in 20 mL HNO_3 65 wt% (Riedel-de Haën, 30709) and 40 mL H_2SO_4 96 wt.% (Merck, 100731) in a 100 mL spherical flask. Solution was stirred for 30 min at ~273 K with an ice-bath. 20 g $KClO_3$ 99+% (Alfa-Aesar, A17075) were gradually added and stirring was continued for 20 h at room temperature (RT). The solution was then added to 200 mL H_2O and GO_1 was obtained by 6 centrifugations (2700 rcf, 5 min) with interval rinsing with H_2O until the pH value of the supernatant solution surpassed 6. GO_1 was air-dried at RT. The same oxidation process was followed for the preparation of sample GO_2 by using 1 g of GO_1 instead of graphite. Oxidation was repeated once more for sample GO_3 by using 0.5 g of GO_2 and half quantities of the rest chemicals as well. The preparation of the GO colloids was performed following our previous method.[S2] Freeze-dried powder from each sample (2 mg) was inserted in a 2 ml polypropylene vial and dispersed in H_2O (0.8 ml) which was pre-adjusted at pH=12.5 (NaOH, 1M). The amount of NaOH used was recorded in order to be taken into consideration later during the determination of the concentration of GO colloids (with TGA). The samples were sonicated (20 min, Branson 2510, 100W, 45 kHz) and left under mild agitation (48 h). Then, the vials were left to stand still and an aliquot from the supernatant was removed (see Table 3 for sampling time) in order to isolate only the fine particles. The sampling times varied, since the GOs with different oxidation degree exhibit different colloidal stability. The lower the oxidation, the less stable the colloid, thus sampling no later than 10 min was necessary for GO_1. For GO_3, sampling at 3 h was sufficient to produce a fine colloid, and in fact with higher concentration than GO_1 (Table S1).

Table S1. Sampling times of the supernatants from the suspensions prepared from the three GO colloids.

	Sampling time	Concentration of GO colloids [mg/ml]
GO_1	10 min	2.2
GO_2	1 h	2.7
GO_3	3h	2.9

2. Z-scan experimental details

The third-order nonlinear optical (NLO) properties and the optical limiting (OL) performance of graphene oxide suspensions have been investigated by means of the Z-scan technique,[S3] using a 35 ps mode locked Nd-YAG laser and a 4 ns Q-switched Nd-YAG laser delivering visible (532 nm) and infrared (1064 nm) laser pulses. The advantage of this technique relies not only on its experimental simplicity (single beam technique), but also because it allows the simultaneous determination, from a single measurement, of the sign and magnitude of the nonlinear absorption and refraction of a sample, which are related to the imaginary and real parts of the third-order susceptibility, $\chi^{(3)}$, respectively. In the Z-scan, the transmittance (T) of a sample is measured as it moves along the propagation direction of a focused Gaussian beam. The sample experiences different light intensity in each position, while around the focal point the intensity is large enough to induce the nonlinear optical response of the material. The measurement of the transmittance of a sample, as it moves along the laser propagation direction of a focused laser beam, is performed by two different ways: (*i*) just after the sample, where the entire transmitted laser light is collected and measured, or (*ii*) after the transmitted laser beam has passed through a small aperture placed in the far field. The former measurement is known as "open-aperture" Z-scan while the latter one as "closed-aperture" Z-scan. From the former measurement, the magnitude of the nonlinear absorption coefficient β of the sample, which is related to the imaginary part of the third-order susceptibility ($\mathrm{Im}\chi^{(3)}$), can be determined by fitting the "open-aperture" Z–scan recording with the following equation:

$$T = \frac{1}{\sqrt{\pi}\left[\dfrac{\beta I_0 L_{eff}}{\left(1+z^2/z_0^2\right)}\right]} \int_{-\infty}^{+\infty} \ln\left[1+\frac{\beta I_0 L_{eff}}{\left(1+z^2/z_0^2\right)}\exp\left(-t^2\right)\right] dt \qquad (1)$$

where T is the normalized transmittance, I_0 is the peak on-axis irradiance of the laser beam at the focus, z_0 is the Reyleigh length and $L_{eff} = [1 - \exp(-\alpha_0 L)]/\alpha_0$ with α_0 being the linear absorption coefficient at the laser wavelength and L denoting the physical length of the sample (*i.e.* the thickness of the cell which was 1 mm). In addition, the presence of a transmittance *minimum* or *maximum* at the "open-aperture" Z-scan recording indicates the sign of the nonlinear absorption coefficient β, corresponding to reverse saturable (RSA, $\beta > 0$) or saturable absorption (SA, $\beta < 0$) respectively.

From the "closed-aperture" Z-scan, the nonlinear refractive parameter γ' of the sample (related to the real part of the third-order susceptibility ($\mathrm{Re}\chi^{(3)}$)) can be determined. A "closed-aperture" Z-scan can exhibit either a pre-focal transmission minimum (valley) followed by a post-focal maximum (peak) or a pre-focal maximum (peak) followed by a post-focal minimum (valley), indicating positive or negative $\mathrm{Re}\chi^{(3)}$, with the sample acting as positive (focusing) or negative (defocusing) lens respectively. The nonlinear refractive parameter γ' can thus be obtained using the following equation:

$$\gamma' = \frac{\lambda\alpha_0}{1-e^{-\alpha_0 L}} \frac{\Delta T_{p-v}}{0.812\pi I_0 \left(1-S\right)^{0.25}} \qquad (2)$$

where λ is the laser wavelength, $\Delta T_{p\text{-}v}$ is the difference between the peak and the valley of the normalized transmittance, S is the linear transmittance of the aperture (defined as $S = 1 - \exp(-2r_a^2/w_a^2)$; with r_a being the radius of the aperture and w_a being the beam radius at the aperture). The quantities α_0, I_0 and L as previously defined.

The NLO parameters γ' and β having been determined, the real and imaginary parts of the third-order susceptibility $\chi^{(3)}$ can be easily calculated according to the following equations:

$$\mathrm{Re}\,\chi^{(3)}\left(esu\right) = \frac{10^{-6} c n_0^2}{480\pi^2}\gamma'\left(cm^2/W\right) \qquad (3a)$$

$$\mathrm{Im}\,\chi^{(3)}\left(esu\right) = \frac{10^{-7} c^2 n_0^2}{96\pi^2\omega}\beta\left(cm/W\right) \qquad (3b)$$

where ω (in s^{-1}) is the frequency of the laser light.

3. UV-Vis-NIR absorption spectra

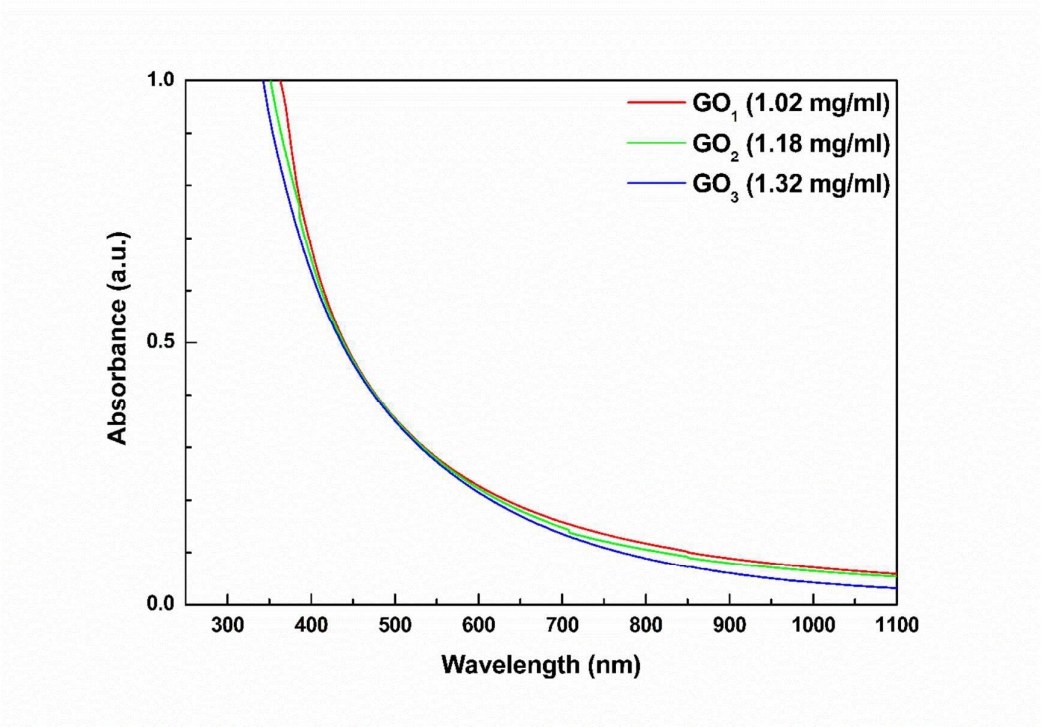

Fig. S1. UV–Vis–NIR spectra of the aqueous GO suspensions with the different degree of oxidation used for the NLO measurements.

4. Dynamic light scattering (DLS) measurements

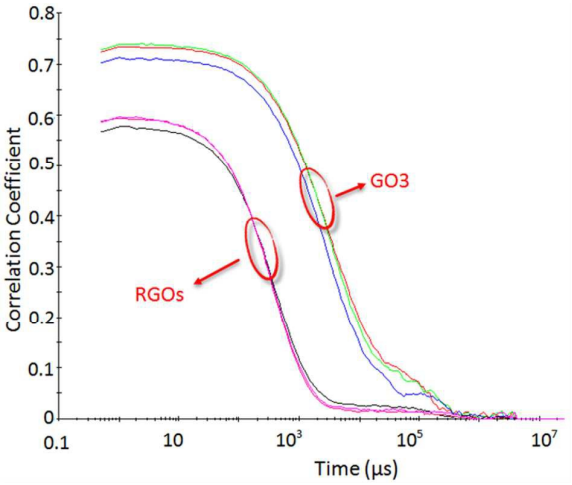

Fig. S2. Autocorrelation functions of several DLS measurements from the stable colloid formed by the highly oxidized GO_3 and the respective results from its reduced derivatives through UV irradiation (RGOs). The latter show faster decay rates manifesting smaller hydrodynamic sizes, i.e., smaller aggregates.

References

S1. (a) D. V. Stergiou, E. K. Diamanti, D. Gournis and M. I. Prodromidis, *Electrochem. Commun.*, 2010, **12**, 1307; (b) R. Y. Gengler, A. Veligura, A. Enotiadis, E. K. Diamanti, D. Gournis, C. Jozsa, B. J. van Wees and P. Rudolf, *Small*, 2010, **6**, 35.

S2. N. Liaros, P. Aloukos, A. Kolokithas-Ntoukas, A. Bakandritsos, T. Szabo, R. Zboril and S. Couris, *J. Phys. Chemi. C*, 2013, **117**, 6842.

S3. M. Sheik-Bahae, A. A. Said, T. H. Wei, D. J. Hagan and E. W. Van Stryland, *IEEE J. Quantum Electron.*, 1990, **26**, 760.